Research Article Vol. 3, No. 2 / February 2016 / Optica 200

Haldane quantum Hall effect for light in a dynamically modulated array of resonators

Momchil Minkov* and Vincenzo Savona

Laboratory of Theoretical Physics of Nanosystems, Ecole Polytechnique Fédérale de Lausanne (EPFL), CH-1015 Lausanne, Switzerland
**Corresponding author: momchil.minkov@epfl.ch*

Received 14 October 2015; revised 12 January 2016; accepted 13 January 2016 (Doc. ID 251916); published 17 February 2016

Topological insulators have attracted abundant attention for a variety of reasons—notably, the possibility for lossless energy transport through edge states "protected" against disorder. Topological effects such as the quantum Hall state can be induced through a gauge field, which is, however, hard to create in practice, especially for charge-neutral particles. One way to induce an effective gauge potential is through a dynamic, time-periodic modulation of the lattice confining such particles. In this way, the Haldane quantum Hall effect was recently observed in a cold-atom system. Here, we show how this same effect can be induced for light confined to a lattice of identical optical resonators, using an on-site modulation of the resonant frequencies. In this system, coupled-mode analysis shows the presence of one-direction edge states immune to backscattering losses. We also discuss possible realizations of the model, which could enable slow-light devices of unprecedented quality.

OCIS codes: (230.4555) Coupled resonators; (230.3240) Isolators; (230.3990) Micro-optical devices.

http://dx.doi.org/10.1364/OPTICA.3.000200

1. INTRODUCTION

Topological order has opened a new frontier in the classification of distinctive phases of matter and is thus a center of attention in theoretical and condensed matter physics [1]. Its study has also reached the field of photonics [2] for two main reasons. First, photonic analogs of topological systems are a promising route to bridging theory and experiment. Second, a signature of a topologically nontrivial material is the presence of one-directional edge states providing energy transport immune to disorder. This could prove extremely valuable for slow-light photonic devices, which find a variety of applications [3,4] but whose performance is severely limited by backscattering due to fabrication imperfections [5–7].

Historically, topological order was first recognized in relation to the quantum Hall effect. In that area, Haldane had a groundbreaking contribution [8] in demonstrating that the effect can arise even with zero magnetic field averaged over a primitive cell. The research into topological photonics was also started by Haldane in two theoretical studies [9,10], which were quickly followed by an experimental realization of a photonic topological insulator using gyromagnetic media [11]. This result was, however, obtained in the gigahertz frequency range. Due to the lack of suitable materials, reproducing this scheme in the visible or the near-infrared spectrum—which are the most interesting for applications—is still a major challenge. The milestone of an experimental realization of topological edge states for light in the near-infrared has been reached using coupled microring resonators [12,13] or coupled waveguides [14] by taking advantage of the symmetry-induced degeneracy of rotating and counter-rotating modes. More specifically, these systems are characterized by a preserved time-reversal symmetry (TRS), which leads to an important limitation of the topological protection. The groundbreaking result (which is now known as the spin quantum Hall effect) of Kane and Mele [15] that, for electrons, this protection is still present in TRS systems relies on the antiunitarity of the time-reversal operator ($T^2 = -1$). For photons, this operator is unitary, and the result no longer holds [2], at least not in its full strength. Instead, the protection relies on the symmetry that prevents the mixing of propagating and counterpropagating modes in a waveguide, which in practice may be broken by disorder. This suggests the need for systems where TRS is broken [9,10,16–23]. Recently, the possibility to use a fine-tuned dynamic modulation of a system to engineer a gauge field for photons has been shown both theoretically [19] and experimentally [24,25].

The seminal work by Haldane [8] considered a honeycomb lattice [Fig. 1(a)] with real first-neighbor and complex second-neighbor couplings. In the absence of the latter, the band structure of the lattice has six Dirac points and no band gap [Fig. 1(b)]. Haldane showed that the complex second-neighbor hopping terms break the TRS and open a topological band gap analogous to the one of a standard quantum Hall system with a constant magnetic field. Generally, complex coupling coefficients on a lattice imply an effective gauge field, with the Peierls phase [26] defining the correspondence between the two. In the Haldane model, the associated magnetic field is zero when averaged over the unit cell, but there is a nonzero magnetic flux through a triangle enclosed by second-neighbor hopping, which is responsible for opening the

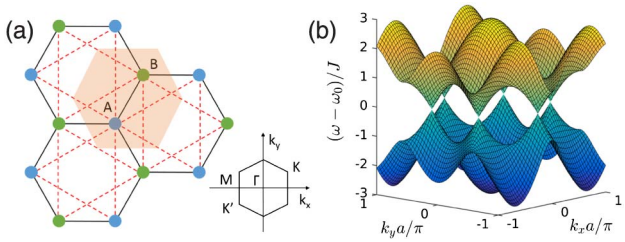

Fig. 1. (a) Honeycomb lattice with two sites A and B in the primitive cell (highlighted in orange). The Haldane model involves a complex second-neighbor hopping, i.e., along the red dashed lines. The Brillouin zone in reciprocal space is also shown. (b) Band structure of the lattice with first-neighbor coupling J and zero second-neighbor coupling. Six Dirac cones at the K-points are present.

band gap. Recently, this was successfully observed using cold atoms in a "shaken" optical lattice [27], which, together with previous research in that field [28–31], inspired the results presented here. In this work, we show how an analog of the Haldane model can be achieved in a Kagomé lattice of photonic resonators using a time-periodic modulation of the resonant frequencies, where only the phase of the modulation varies among different sites, in a spatially periodic manner. We further show the existence of backscattering-immune edge states and discuss the possibilities for a practical implementation of the system.

2. MODEL

We consider a lattice of optical resonators in which the resonant frequencies ω_i are subject to a periodic modulation in time. The linear photonic Hamiltonian, most generally, reads

$$H=\sum_i(\omega_i+A_i\cos(\Omega t+\phi_i))a_i^\dagger a_i-\sum_{ij}J_{ij}a_i^\dagger a_j, \tag{1}$$

where $a^\dagger$ is the photon creation operator, J_{ij} are the hopping coefficients, and A_i and ϕ_i denote the site-dependent amplitude and phase of the dynamic modulation, which can be achieved, for example, through electro-optic modulation [32,33], optically induced material nonlinearities [34], or optomechanical interaction with phonon modes [35]. The Hamiltonian is particle-number preserving; thus Eq. (1) describes the system with any fixed number of photons (subspaces of different photon numbers are decoupled). The equation also applies to classical light, since it is a concise way to write the coupled-mode theory that can be used for an array of optical resonators. In Supplement 1, we outline the theoretical details of the Floquet theory [36–38] that we employ to solve the time-periodic Hamiltonian of Eq. (1). One approach is to expand the modes of the array on the Floquet basis:

$$|\{n_i\},m\rangle=|\{n_i\}\rangle\exp\left(-\frac{i}{\Omega}\sum_i A_i\sin(\Omega t+\phi_i)n_i+im\Omega t\right), \tag{2}$$

where n_i denotes the occupation number of site i, and m is an integer. In Supplement 1, we derive the matrix elements of the matrix for diagonalization whose eigenstates correspond to the exact solution of the system when all orders m are included. In practice, we truncate m up to a given $m_{\max}$, always checking for convergence. The relationship between this system and the Haldane model is more intuitively revealed through Floquet perturbation theory, which is also outlined in detail in Supplement 1. Within this approach, a time-independent effective Hamiltonian describing the evolution of the system for timescales much larger than $1/\Omega$ can be written and expanded in orders of $1/\Omega$. To first order, this results in effective *complex* coupling coefficients $J'_{ij}+iJ''_{ij}$, where

$$J'_{ij}=J_{ij}\mathcal{J}_0(\rho_{ij}), \tag{3}$$

$$J''_{ij}=2\sum_{ij}\sum_{m=1}^{\infty}\frac{(-1)^m}{\Omega m}\sum_p\mathcal{J}_m(\rho_{ip})\mathcal{J}_m(\rho_{pj})J_{ip}J_{pj}\times\sin(m(\phi_{ip}-\phi_{pj}))a_i^\dagger a_j, \tag{4}$$

with $\mathcal{J}_m$ the Bessel functions of the first kind, and ρ_{ij},ϕ_{ij} constants defined as

$$\rho_{ij}e^{i\phi_{ij}}=(A_je^{i\phi_j}-A_ie^{i\phi_i})/\Omega. \tag{5}$$

The imaginary iJ''_{ij} thus introduces a gauge field for the photons, and more specifically—in the lattice geometries we discuss below—the magnetic flux required for the Haldane effect.

In the recent experimental observation of the Haldane model with cold atoms [27], the honeycomb lattice confining the atoms was "shaken" by a periodic, elliptical modulation. In the reference frame of the lattice, this results in a site-dependent potential in the Hamiltonian. This can also be implemented in the resonator array considered here through a modulation of the form of Eq. (1), with the remark that, since both our Hamiltonian and that of Ref. [27] are particle-number preserving, the particle statistics (bosons or fermions) are not important. Thus, all the considerations of Ref. [27] also hold for the lattice of optical resonators if we set the couplings J_{ij} of Eq. (1) to those of the honeycomb lattice, and A_i and ϕ_i such that

$$A_i\cos(\Omega t+\phi_i)=A_0\frac{x_i}{r}\cos(\Omega t)+A_0\frac{y_i}{r}\sin(\Omega t),\qquad\forall\ i. \tag{6}$$

Here, A_0 is a constant, (x_i,y_i) is the position of the ith resonator, and r is the first-neighbor distance. Thus, replicating the cold-atom system is possible. However, we note that this requires a gradient in the amplitude A_i of the modulation of the frequency of the optical resonators. This is because, in the cold-atom case, there is a constant inertial force on all lattice sites, and thus a spatial gradient in the potential. Ideally, we would like to have instead a modulation that shares the spatial periodicity of the underlying lattice. This is, however, impossible in the case of the honeycomb geometry, for the following reason. The lattice has two sites in the unit cell [marked A and B in Fig. 1(a)]. Assuming a modulation with the same periodicity, we are limited to two arbitrary amplitudes A_A and A_B, and two arbitrary phases φ_A, φ_B. Whatever their values, however, looking at Eq. (5), it is obvious that $\phi_{AB}=\pi+\phi_{BA}$, which means that $\phi_{AB}-\phi_{BA}=\pi$. Since all terms in the second-neighbor imaginary hoppings [Eq. (4)] that come out of this modulation are proportional to $\sin(m(\phi_{AB}-\phi_{BA}))$ with m an integer, they are all zero.

The spatial gradient in A_i that is needed in the honeycomb geometry breaks the spatial periodicity and makes it impossible to analyze the system in momentum space, which is a significant theoretical disadvantage. In addition, in view of potential experimental realizations, this feature introduces an extra challenge, since the maximum amplitude of the modulation is inevitably

limited, which in turn would limit the maximum system size. Fortunately, this can be easily overcome through a small modification of the lattice geometry—namely, by considering the Kagomé lattice illustrated in Fig. 2(a). This lattice has three lattice sites per elementary cell, and the band structure [Fig. 2(b)] is similar to that of the honeycomb lattice in that there are six Dirac cones. The main difference comes from the additional flat band. Importantly, in the presence of second-neighbor couplings similar to those of the Haldane model, topologically nontrivial band gaps can be opened between the first and the second and/or the second and the third bands [39,40].

We thus now focus on a Kagomé lattice of identical resonators of frequency ω_0 on all sites, assuming first-neighbor couplings only [along the black lines of Fig. 2(a)], with a hopping coefficient J. The dynamic modulation that we additionally assume has the form $\omega_A = \omega_0 + A_0\cos(\Omega t + \varphi)$, $\omega_B = \omega_0 + A_0\cos(\Omega t + 2\varphi)$, and $\omega_C = \omega_0 + A_0\cos(\Omega t + 3\varphi)$, where A, B, and C refer to the three sites of the primitive cell. Since the Hamiltonian is time-periodic, the spectrum has a Brillouin-zone-like structure in the sense that, if ω is an eigenstate of the time-dependent Hamiltonian, so are $\omega + m\Omega$, for all integer m. The eigenstates are time-periodic functions with period T, and can be computed through expansion on the Floquet basis of Eq. (2). We consider the subspace of a single excitation only, i.e., $n_i = 1$, $n_{j\neq i} = 0$, and truncate the orders of m at $m_{\max} = 10$ (convergence is always checked).

The Floquet two-dimensional band structure of the lattice can then also be computed, with time- and space-periodic solutions

$$u_n(\mathbf{k}, t) = \sum_{i,m} v_{i,m}(\mathbf{k}, n) e^{-i\mathbf{k}\mathbf{R}_i} e^{im\Omega t}, \tag{7}$$

with $v_{i,m}(\mathbf{k}, n)$ the eigenvectors from the diagonalization, and $\mathbf{R}_i$ the position of site i. The Floquet band diagram is shown in Figs. 3(a) and 3(b) for $J = 0.1\Omega$, $A_0 = 0.9\Omega$, and $\varphi = 2.1$. As discussed and displayed in Fig. 3(a), the bands are repeated in frequency space at an interval of Ω. In Fig. 3(b), which shows a close-up of the zeroth-order bands of Fig. 3(a), we see that band gaps are opened due to the dynamic modulation. To quantify their topological properties, we compute the Chern number

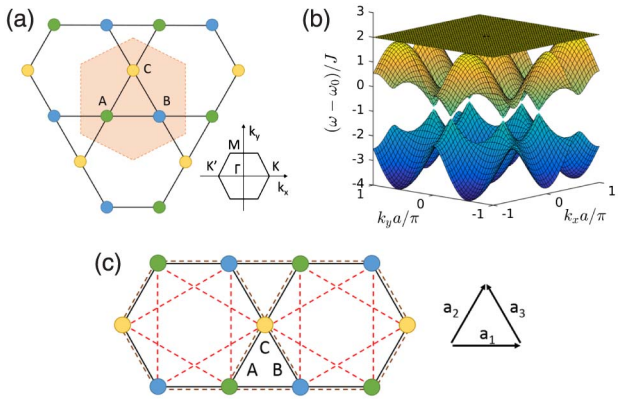

Fig. 2. (a) Kagomé lattice with three sites in the primitive cell, and the corresponding Brillouin zone. (b) Corresponding band structure with first-neighbor coupling J. There are six Dirac cones, and in addition a flat band. (c) The dynamic modulation results in effective imaginary couplings along the dashed lines. These are both first- and second-neighbor (brown and red lines, respectively). The three first-neighbor vectors a_1, a_2, and a_3 appearing in Eq. (11) are also defined.

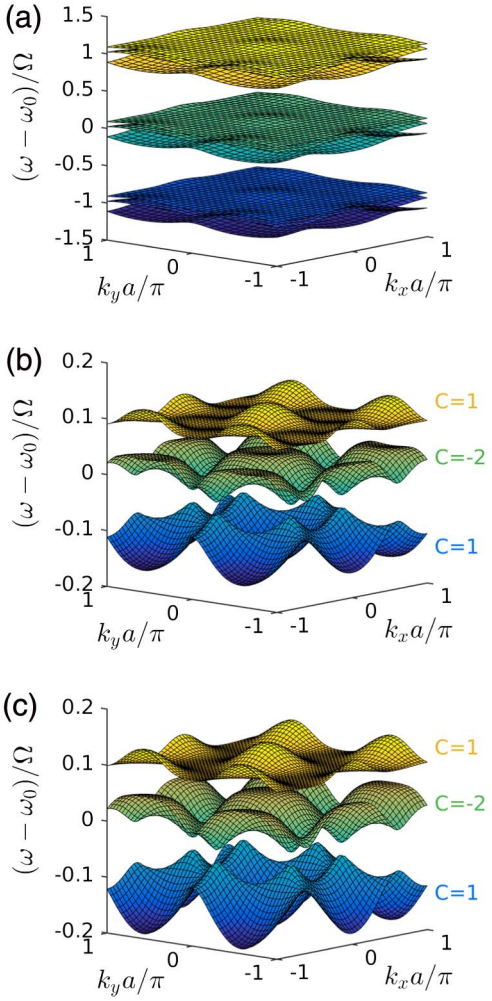

Fig. 3. (a) Quasi-energy bands computed through diagonalization on the Floquet basis, for $J = 0.1\Omega$, $A_0 = 0.9\Omega$, and $\varphi = 2.1$. The bands are repeated in orders of $m\Omega$, with m an integer. (b) Zoom-in on the $m = 0$ region of (a). (c) Bands computed through a perturbative expansion of the effective time-independent Hamiltonian. In (b) and (c), the Chern number for each band is indicated.

for all bands by integrating the Berry curvature $\mathcal{F}(\mathbf{k})$ [41,42] over the Brillouin zone. Numerically, we compute $\mathcal{F}(\mathbf{k})$ on a discrete mesh in $\mathbf{k}$-space using the eigenvectors $v_{m,i}(\mathbf{k}, n)$ [43,44]. The nonzero Chern numbers (1, –2, and 1 for the three bands, respectively) confirm the nontrivial nature of the band gaps.

The band structure can also be computed starting from the perturbative expansion of Eq. (1). As mentioned above, this has the advantage of making the connection between this system and the Haldane model more intuitive. In the presence of the modulation, the effective Hamiltonian up to first order in perturbation theory can then be written in k-space as

$$\tilde{H} = \sum_{\mathbf{k}} \mathcal{A}^{\dagger}_{\mathbf{k}}(\omega_0 + \mathcal{H}(\mathbf{k}))\mathcal{A}_{\mathbf{k}} \tag{8}$$

with

$$\mathcal{A}^{\dagger}_{\mathbf{k}} = (a^{\dagger}_{A,\mathbf{k}}, a^{\dagger}_{B,\mathbf{k}}, a^{\dagger}_{C,\mathbf{k}}), \tag{9}$$

where $a^{\dagger}_{A,\mathbf{k}}$ is the Fourier transform of the $a^{\dagger}_A$ operator creating a particle on site A, and correspondingly for B and C. The coupling matrix is given by

$$\mathcal{H}(\mathbf{k}) = -2J \begin{pmatrix} 0 & t_{AB}(\mathbf{k}) & t_{AC}(\mathbf{k}) \\ t_{AB}^*(\mathbf{k}) & 0 & t_{BC}(\mathbf{k}) \\ t_{AC}^*(\mathbf{k}) & t_{BC}^*(\mathbf{k}) & 0 \end{pmatrix}, \quad (10)$$

where the (dimensionless) couplings can be split into

$$\begin{aligned} t_{AB}(\mathbf{k}) &= (t_{AB,0} + t_{AB,1})\cos(\mathbf{k}\mathbf{a}_1) + t'_{AB,1}\cos(\mathbf{k}(\mathbf{a}_2 + \mathbf{a}_3)), \\ t_{AC}(\mathbf{k}) &= (t_{AC,0} + t_{AC,1})\cos(\mathbf{k}\mathbf{a}_2) + t'_{AC,1}\cos(\mathbf{k}(\mathbf{a}_1 - \mathbf{a}_3)), \\ t_{BC}(\mathbf{k}) &= (t_{BC,0} + t_{BC,1})\cos(\mathbf{k}\mathbf{a}_2) + t'_{BC,1}\cos(\mathbf{k}(\mathbf{a}_1 + \mathbf{a}_2)), \end{aligned} \quad (11)$$

where, in the first line, $t_{AB,0}$ is the first-neighbor coupling from site A to site B, $t_{AB,1}$ is the double-hop coupling (through site C) to a first-neighbor site B, and $t'_{AB,1}$ is the double-hop coupling (again through site C, but in a different direction) to a second-neighbor site B. The vectors $\mathbf{a}_i$ are defined such that $\mathbf{a}_1$ points from A to B, $\mathbf{a}_2$ points from A to C, and $\mathbf{a}_3$ points from B to C [see Fig. 2(c)]. Simply put, the zeroth-order effective Hamiltonian results in rescaled first-neighbor couplings [$t_{AB,0}$, $t_{AC,0}$, $t_{BC,0}$, black lines in Fig. 2(c)], while the first order results in all the couplings marked by dashed lines in Fig. 2(c) ($t_{AB,1}$, $t_{AC,1}$, $t_{BC,1}$, brown lines; $t'_{AB,1}$, $t'_{AC,1}$, $t'_{BC,1}$, red lines), which always involve an intermediate hopping, and are purely imaginary. The coefficients can be derived from Eqs. (3) and (4), and are given explicitly in Supplement 1. In Fig. 3(c), we show the bands computed by diagonalizing this effective Hamiltonian, which agree very well with the exact solution of Fig. 3(b), and the computed Chern numbers are the same.

3. EDGE STATES

Topological invariants like the Chern number cannot change as long as the band gap remains open. Hence, the width of the band gap is an important parameter, giving an energy scale to the topological protection against disorder (only fluctuations on a larger scale can destroy the topological properties). Thus, in Fig. 4, we plot maps of the gap width Δ_T (if two gaps are present, the largest value is taken), versus the parameters A_0 and φ. The data in Figs. 4(a) and 4(b) are computed for $J = 0.1\Omega$, with the perturbation theory Hamiltonian in Fig. 4(a), and the full diagonalization in Fig. 4(b), and show very good agreement. In Figs. 4(c) and 4(d), $J = 0.5\Omega$ was used, and the agreement is no longer present. It is natural that the perturbative expansion works well for small J/Ω when the Floquet bands of different orders are well-separated [Fig 3(a)], but has limited reliability as J increases. Importantly, however, the topological effect is present even beyond perturbation theory: a gap of width larger than 0.2Ω is opened for $J = 0.5\Omega$, $A_0 = 1.6\Omega$, and $\varphi = 2.1$. Notice that for any value of the parameters in this system, the band gap is inevitably limited to a fraction of Ω due to the higher-order Floquet bands.

In Fig. 5, we show the band structures with the largest band gaps for $J = 0.3\Omega$, $J = 0.5\Omega$, and $J = 0.7\Omega$, with parameters A_0 and φ chosen for the largest Δ_T (see Fig. 2 of Supplement 1). Topologically, there is a difference between the bands in Figs. 3(b) and 5(a), with Chern numbers 1, −2, and 1, and those of Figs. 5(b) and 5(c), with Chern numbers 1, 0, and −1. What is important, however, is that in both cases there are bands with a nonzero topological invariant. The bulk-boundary correspondence principle [1,2] then applies, guaranteeing the existence

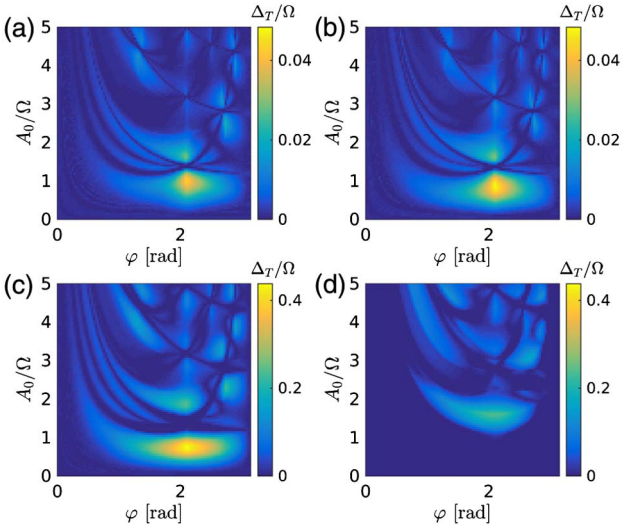

Fig. 4. (Largest) width of the opened band gap due to the dynamic modulation of frequency Ω versus the amplitude A_0 and the phase angle φ for the Kagomé lattice with first-neighbor coupling $J = 0.1\Omega$. (a) Floquet perturbation theory. (b) Expansion on the Floquet basis. (c),(d) Same as (a) and (b), but for $J = 0.5\Omega$. The color scheme is the same in panels (a) and (b), as well as in panels (c) and (d).

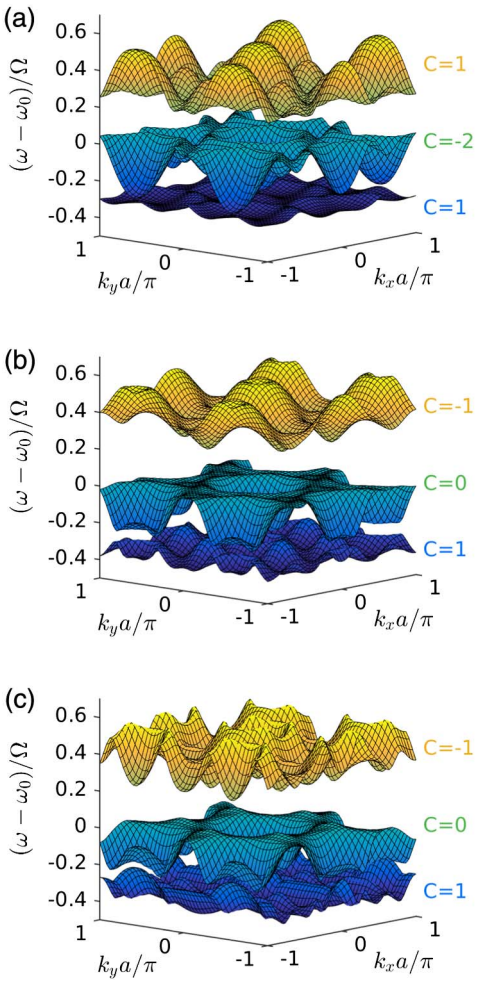

Fig. 5. Bands structure with the largest possible band gap for various values of J/Ω. (a) $J = 0.3\Omega$, $A_0 = 0.5\Omega$, and $\varphi = 2.1$. (b) $J = 0.5\Omega$, $A_0 = 1.6\Omega$, and $\varphi = 2.1$. (c) $J = 0.7\Omega$, $A_0 = 3.05\Omega$, and $\varphi = 2.67$. The Chern number for each band is indicated.

of gapless edge states at an interface between the topological material and a topologically trivial one (e.g., empty space). In terms of practical applications, propagating modes robust to disorder are thus expected to appear in a finite system.

The existence of the topological edge modes is illustrated in Fig. 6 for a ribbon geometry, with a finite number of sites in one direction, and periodic boundary conditions in the other. The one-dimensional Floquet band structure can again be computed by expanding on the Floquet basis, and is shown in Figs. 6(a) and 6(d) for $J = 0.5\Omega$, $A_0 = 1.6\Omega$, and $\varphi = 2.1$. The difference between the two panels comes from the truncation at the edges—compare Figs. 6(b) and 6(e). Regardless of how we truncate, there is a band that closes the band gap of the bulk structure, due to the nonzero topological invariants. Modes belonging to that band are localized close to the boundaries of the ribbon; the important point, however, is that the modes at k_x and $-k_x$ are localized at opposite edges. This is illustrated in Figs. 6(c) and 6(f), where we plot the position dependence of the magnitude of the eigenvectors of the two states indicated by a blue and a red dot in Figs. 6(a) and 6(d), respectively. The amplitude on the x axis is the quantity $\sum |v_{m,i}(\mathbf{k}, n)|^2$, where the sum is over all m, and over all sites at the same position along y. The edge modes are exponentially localized at the boundaries [notice the logarithmic scale on the x axes of Figs. 6(c) and 6(f)]; thus the overlap between the forward- and backward-propagating modes decreases exponentially with the width of the ribbon in the y direction.

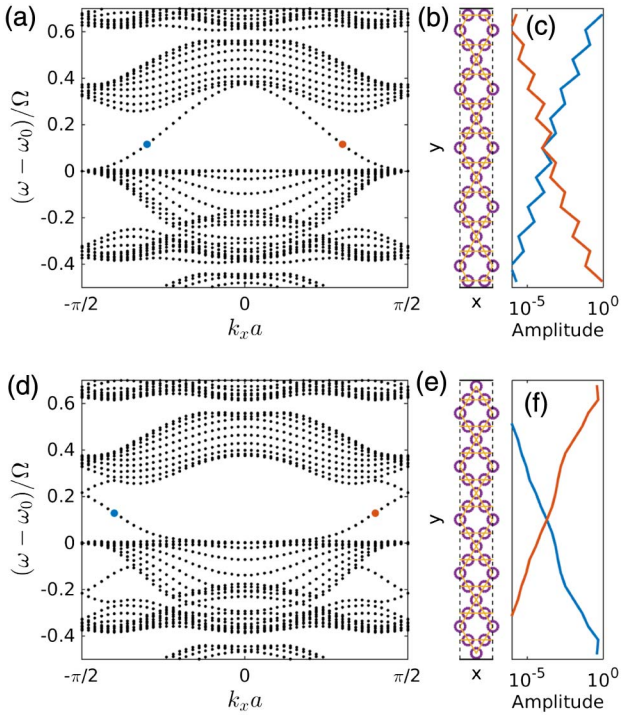

Fig. 6. (a) Floquet bands for the ribbon geometry shown in (b), with a finite number of sites in one direction (the system is truncated at the solid black lines), and periodic boundary conditions in the other (along the dashed black lines). The parameters are as in Fig. 4(b): $J = 0.5\Omega$, $A_0 = 1.6\Omega$, and $\phi = 2.1$. (c) Spatial dependence of the eigenstates marked in blue and red, respectively, in panel (a). The y axis is aligned with the y axis of panel (b). (d)–(f) Same as (a)–(c), but for a different truncation [compare (b) and (e)].

This is only possible due to the broken TRS, and ensures protection against backscattering in the presence of disorder.

4. DISCUSSION

Our proposal is related to the seminal work of Ref. [19], in which a dynamic modulation of an optical lattice was first proposed to achieve an effective gauge field for photons. On the fundamental level, the main difference here is the lattice geometry, which is such that a *second-neighbor* complex coupling is sufficient to give rise to the quantum Hall effect (as in the Haldane model). On the practical side, this actually leads to a variety of simplifications, perhaps most importantly the fact that the resonant frequency of each individual cavity has to be modulated, instead of the cavity–cavity coupling coefficients. To achieve the latter, in Ref. [19] a fairly complex coupling scheme was proposed, in which two different resonators couple through an intermediate "link" cavity, with specific requirements for the symmetries of all cavity modes. Our system is instead the simplest possible, consisting of an array of *identical, single-mode* resonators. Furthermore, the dynamic modulation itself takes the simple form of a *constant amplitude* across the whole system, and a *spatially periodic* phase pattern.

Several considerations have to be made for the results presented here to have practical implications. We have not considered the loss rate κ of the optical resonators, which is in practice always nonzero. To be able to meaningfully talk about light transport, this must be smaller than the coupling constant J. In addition, κ must also be smaller than the band gap Δ_T, so that the latter can be resolved. By extension, this also implies $\kappa \ll \Omega$. In state-of-the-art photonic crystal cavities, κ/ω_0 of the order of 10^{-6} can now be routinely achieved [45–47] at telecommunication frequencies $\omega_0/2\pi \approx 200$ THz; thus $\kappa/2\pi = 0.5$ GHz is a reasonable and conservative assumption. The coupling constant J is the easiest parameter to control by varying the distance between resonators. Thus the most important challenge is to have a sufficiently high Δ_T. In fact, independently of κ, Δ_T is a general figure of merit for the magnitude of the topological protection that should be maximized.

In Ref. [19], electro-optic modulation was suggested as the practical tool for driving the resonant-frequency oscillation. This offers sufficient control over the phase, and has been shown to be scalable [19,48]. The maximum achievable modulation frequency $\Omega/2\pi$ is of the order of several gigahertz. A band gap Δ_T of the order of 1 GHz could thus be achieved, which lies just above the limit set by κ. We note that this challenge holds both for our proposal and for that of Ref. [19]. Very recently [22], it was suggested to use the coupling of the optical resonators to localized phonon modes to induce the frequency modulation. In this scheme, Ω is fixed by the phonon resonant frequency, which can be as high as $\Omega/2\pi = 10$ GHz in two-dimensional optomechanical crystals [49]. This is sufficiently large for our scheme, and the required phase control can be easily implemented through the phase of the lasers driving the mechanical oscillations [22,35]. Within that paradigm, another recent optomechanical scheme [23] investigated the Kagomé lattice of resonators, focusing on creating and probing topological states for sound (i.e., phonons). Within that proposal, it is also possible to create topological states of light, but the size of the band gap is shown to be proportional to the phonon hopping coefficient. This is typically orders of magnitude smaller than the phonon resonant frequency,

and thus also smaller than the best optical loss rate κ that could possibly be achieved in state-of-the-art photonic devices.

While both of the modulation schemes mentioned above could be employed for an experimental realization of our system, a third option is also worth mentioning. Using the optically induced Kerr nonlinearity, repeated switching at a terahertz rate has recently been demonstrated in a micropillar cavity [34]. The maximum amplitude in such a scheme is limited to only a fraction of Ω, but assuming $\Omega/2\pi = 1$ THz, $A_0 = 0.05\Omega$ (which can be read out of the sine-like dependence of the cavity resonant frequency measured in Ref. [34]), $J = 0.2\Omega$, and $\varphi = 2.1$, we obtain for our Kagomé lattice a topological band gap of width 0.033Ω, i.e., $\Delta_T/2\pi = 33$ GHz. This value is two orders of magnitude larger than the loss rate of state-of-the-art cavities, which ensures that the band gap cannot be closed by the dephasing associated to the radiative losses. Regarding disorder, the nonzero topological invariants guarantee protection when the energy scale associated to the disorder magnitude is much smaller than Δ_T. Disorder in photonic systems is a complex phenomenon and appears in various forms—thus, a comprehensive study would require intricate modeling and is beyond the scope of this work. However, we note that the Δ_T value we estimate here is very similar to the magnitude of the disorder-induced fluctuation in the resonant frequencies of nominally identical photonic crystal cavities [50,51]. Moreover, the latter can in principle be further reduced by post-processing techniques [52,53]. All these considerations suggest that an implementation of our scheme on a photonic crystal platform is a very promising outlook for future research.

In conclusion, we have described a straightforward implementation of the Haldane-like quantum Hall effect for light in a lattice of optical cavities, with an effective gauge field produced through a time-periodic modulation of the resonant frequencies. The site dependence of the phase of the modulation breaks TRS and opens topologically nontrivial band gaps, which, in a finite geometry, yields propagating, backscattering-free edge states. These can find applications for high bit-rate storage [4]; for enhanced nonlinear effects, e.g., for frequency conversion or generation of nonclassical light for quantum information processing [54–57]; and for enhanced radiative coupling between distant quantum dots for on-chip quantum computation [58,59].

Funding. Schweizerischer Nationalfonds zur Förderung der Wissenschaftlichen Forschung (SNF) (200020_149537).

Acknowledgment. We thank Hugo Flayac for discussions and Willem Vos for highlighting the relevance of Ref. [34].

See Supplement 1 for supporting content.

REFERENCES

1. M. Z. Hasan and C. L. Kane, "Colloquium: topological insulators," Rev. Mod. Phys. **82**, 3045–3067 (2010).
2. L. Lu, J. D. Joannopoulos, and M. Soljačić, "Topological photonics," Nat. Photonics **8**, 821–829 (2014).
3. T. F. Krauss, "Why do we need slow light?" Nat. Photonics **2**, 448–450 (2008).
4. T. Baba, "Slow light in photonic crystals," Nat. Photonics **2**, 465–473 (2008).
5. S. John, "Strong localization of photons in certain disordered dielectric superlattices," Phys. Rev. Lett. **58**, 2486–2489 (1987).
6. M. Patterson, S. Hughes, S. Combrié, N. V. Q. Tran, A. De Rossi, R. Gabet, and Y. Jaouën, "Disorder-induced coherent scattering in slow-light photonic crystal waveguides," Phys. Rev. Lett. **102**, 1–4 (2009).
7. S. Mazoyer, J. P. Hugonin, and P. Lalanne, "Disorder-induced multiple scattering in photonic-crystal waveguides," Phys. Rev. Lett. **103**, 063903 (2009).
8. F. D. M. Haldane, "Model for a quantum Hall effect without Landau levels: condensed-matter realization of the 'parity anomaly'," Phys. Rev. Lett. **61**, 2015–2018 (1988).
9. F. Haldane and S. Raghu, "Possible realization of directional optical waveguides in photonic crystals with broken time-reversal symmetry," Phys. Rev. Lett. **100**, 013904 (2008).
10. S. Raghu and F. D. M. Haldane, "Analogs of quantum-Hall-effect edge states in photonic crystals," Phys. Rev. A **78**, 033834 (2008).
11. Z. Wang, Y. Chong, J. D. Joannopoulos, and M. Soljačić, "Observation of unidirectional backscattering-immune topological electromagnetic states," Nature **461**, 772–775 (2009).
12. M. Hafezi, E. A. Demler, M. D. Lukin, and J. M. Taylor, "Robust optical delay lines with topological protection," Nat. Phys. **7**, 907–912 (2011).
13. M. Hafezi, S. Mittal, J. Fan, A. Migdall, and J. M. Taylor, "Imaging topological edge states in silicon photonics," Nat. Photonics **7**, 1001–1006 (2013).
14. M. C. Rechtsman, J. M. Zeuner, Y. Plotnik, Y. Lumer, D. Podolsky, F. Dreisow, S. Nolte, M. Segev, and A. Szameit, "Photonic Floquet topological insulators," Nature **496**, 196–200 (2013).
15. C. L. Kane and E. J. Mele, "Quantum spin Hall effect in graphene," Phys. Rev. Lett. **95**, 226801 (2005).
16. J. Koch, A. A. Houck, K. L. Hur, and S. M. Girvin, "Time-reversal-symmetry breaking in circuit-QED-based photon lattices," Phys. Rev. A **82**, 1–18 (2010).
17. R. O. Umucalılar and I. Carusotto, "Artificial gauge field for photons in coupled cavity arrays," Phys. Rev. A **84**, 043804 (2011).
18. R. O. Umucalılar and I. Carusotto, "Fractional quantum Hall states of photons in an array of dissipative coupled cavities," Phys. Rev. Lett. **108**, 206809 (2012).
19. K. Fang, Z. Yu, and S. Fan, "Realizing effective magnetic field for photons by controlling the phase of dynamic modulation," Nat. Photonics **6**, 782–787 (2012).
20. M. Hafezi and P. Rabl, "Optomechanically induced non-reciprocity in microring resonators," Opt. Express **20**, 7672–7684 (2012).
21. S. Longhi, "Effective magnetic fields for photons in waveguide and coupled resonator lattices," Opt. Lett. **38**, 3570–3573 (2013).
22. M. Schmidt, S. Kessler, V. Peano, O. Painter, and F. Marquardt, "Optomechanical creation of magnetic fields for photons on a lattice," Optica **2**, 635–641 (2015).
23. V. Peano, C. Brendel, M. Schmidt, and F. Marquardt, "Topological phases of sound and light," Phys. Rev. X **031011**, 1–18 (2015).
24. K. Fang, Z. Yu, and S. Fan, "Photonic Aharonov-Bohm effect based on dynamic modulation," Phys. Rev. Lett. **108**, 1–5 (2012).
25. L. D. Tzuang, K. Fang, P. Nussenzveig, S. Fan, and M. Lipson, "Non-reciprocal phase shift induced by an effective magnetic flux for light," Nat. Photonics **8**, 701–705 (2014).
26. R. Peierls, "On the theory of the diamagnetism of conduction electrons," Z. Phys. **80**, 763–791 (1933).
27. G. Jotzu, M. Messer, R. Desbuquois, M. Lebrat, T. Uehlinger, D. Greif, and T. Esslinger, "Experimental realisation of the topological Haldane model," Nature **515**, 237–240 (2014).
28. A. Eckardt, P. Hauke, P. Soltan-Panahi, C. Becker, K. Sengstock, and M. Lewenstein, "Frustrated quantum antiferromagnetism with ultracold bosons in a triangular lattice," Europhys. Lett. **89**, 10010 (2010).
29. P. Hauke, O. Tieleman, A. Celi, C. Ölschläger, J. Simonet, J. Struck, M. Weinberg, P. Windpassinger, K. Sengstock, M. Lewenstein, and A. Eckardt, "Non-Abelian gauge fields and topological insulators in shaken optical lattices," Phys. Rev. Lett. **109**, 1–6 (2012).
30. J. Struck, C. Olschläger, M. Weinberg, P. Hauke, J. Simonet, A. Eckardt, M. Lewenstein, K. Sengstock, and P. Windpassinger, "Tunable gauge potential for neutral and spinless particles in driven optical lattices," Phys. Rev. Lett. **108**, 1–5 (2012).
31. N. Goldman and J. Dalibard, "Periodically driven quantum systems: effective Hamiltonians and engineered gauge fields," Phys. Rev. X **4**, 031027 (2014).

32. Q. Xu, B. Schmidt, S. Pradhan, and M. Lipson, "Micrometre-scale silicon electro-optic modulator," Nature **435**, 325–327 (2005).
33. Y.-H. Kuo, Y. K. Lee, Y. Ge, S. Ren, J. E. Roth, T. I. Kamins, D. A. B. Miller, and J. S. Harris, "Strong quantum-confined Stark effect in germanium quantum-well structures on silicon," Nature **437**, 1334–1336 (2005).
34. E. Yüce, G. Ctistis, J. Claudon, E. Dupuy, R. D. Buijs, B. de Ronde, A. P. Mosk, J. Gérard, and W. L. Vos, "All-optical switching of a microcavity repeated at terahertz rates," Opt. Lett. **38**, 374–376 (2013).
35. M. Aspelmeyer, T. J. Kippenberg, and F. Marquardt, "Cavity optomechanics," Rev. Mod. Phys. **86**, 1391–1452 (2014).
36. J. H. Shirley, "Solution of the Schrödinger equation with a Hamiltonian periodic in time," Phys. Rev. **138**, B979–B987 (1965).
37. H. Sambe, "Steady states and quasienergies of a quantum-mechanical system in an oscillating field," Phys. Rev. A **7**, 2203–2213 (1973).
38. A. Eckardt, C. Weiss, and M. Holthaus, "Superfluid-insulator transition in a periodically driven optical lattice," Phys. Rev. Lett. **95**, 1–4 (2005).
39. K. Ohgushi, S. Murakami, and N. Nagaosa, "Spin anisotropy and quantum Hall effect in the kagomé lattice: chiral spin state based on a ferromagnet," Phys. Rev. B **62**, R6065–R6068 (2000).
40. H. M. Guo and M. Franz, "Topological insulator on the kagome lattice," Phys. Rev. B **80**, 113102 (2009).
41. M. V. Berry, "Quantal phase factors accompanying adiabatic changes," Proc. R. Soc. London Ser. A **392**, 45–57 (1984).
42. J. Zak, "Berry's phase for energy bands in solids given the adiabatic form," Phys. Rev. Lett. **62**, 2747–2750 (1989).
43. R. Resta, "Manifestations of Berry's phase in molecules and condensed matter," J. Phys. **12**, R107–R143 (2000).
44. A. Soluyanov, "Topological aspects of band theory," Ph.D. thesis (The State University of New Jersey, 2012).
45. M. Notomi, E. Kuramochi, and T. Tanabe, "Large-scale arrays of ultrahigh-Q coupled nanocavities," Nat. Photonics **2**, 741–747 (2008).
46. Y. Lai, S. Pirotta, G. Urbinati, D. Gerace, M. Minkov, V. Savona, A. Badolato, and M. Galli, "Genetically designed L3 photonic crystal nanocavities with measured quality factor exceeding one million," Appl. Phys. Lett. **104**, 241101 (2014).
47. H. Sekoguchi, Y. Takahashi, T. Asano, and S. Noda, "Photonic crystal nanocavity with a q-factor of 9 million," Opt. Express **22**, 916–924 (2014).
48. H. Lira, Z. Yu, S. Fan, and M. Lipson, "Electrically driven nonreciprocity induced by interband photonic transition on a silicon chip," Phys. Rev. Lett. **109**, 1–5 (2012).
49. A. H. Safavi-Naeini, J. T. Hill, S. Meenehan, J. Chan, S. Gröblacher, and O. Painter, "Two-dimensional phononic-photonic band gap optomechanical crystal cavity," Phys. Rev. Lett. **112**, 153603 (2014).
50. H. Hagino, Y. Takahashi, Y. Tanaka, T. Asano, and S. Noda, "Effects of fluctuation in air hole radii and positions on optical characteristics in photonic crystal heterostructure nanocavities," Phys. Rev. B **79**, 085112 (2009).
51. M. Minkov, U. P. Dharanipathy, R. Houdré, and V. Savona, "Statistics of the disorder-induced losses of high-q photonic crystal cavities," Opt. Express **21**, 28233–28245 (2013).
52. F. Intonti, N. Caselli, S. Vignolini, F. Riboli, S. Kumar, A. Rastelli, O. G. Schmidt, M. Francardi, A. Gerardino, L. Balet, L. H. Li, A. Fiore, and M. Gurioli, "Mode tuning of photonic crystal nanocavities by photoinduced non-thermal oxidation," Appl. Phys. Lett. **100**, 033116 (2012).
53. A. Y. Piggott, K. G. Lagoudakis, T. Sarmiento, M. Bajcsy, G. Shambat, and J. Vučković, "Photo-oxidative tuning of individual and coupled gas photonic crystal cavities," Opt. Express **22**, 15017–15023 (2014).
54. B. Corcoran, C. Monat, C. Grillet, D. J. Moss, B. J. Eggleton, T. P. White, L. O'Faolain, and T. F. Krauss, "Green light emission in silicon through slow-light enhanced third-harmonic generation in photonic-crystal waveguides," Nat. Photonics **3**, 206–210 (2009).
55. C. Monat, M. Ebnali-Heidari, C. Grillet, B. Corcoran, B. J. Eggleton, T. P. White, L. O'Faolain, J. Li, and T. F. Krauss, "Four-wave mixing in slow light engineered silicon photonic crystal waveguides," Opt. Express **18**, 22915–22927 (2010).
56. S. Azzini, D. Grassani, M. J. Strain, M. Sorel, L. G. Helt, J. E. Sipe, M. Liscidini, M. Galli, and D. Bajoni, "Ultra-low power generation of twin photons in a compact silicon ring resonator," Opt. Express **20**, 23100–23107 (2012).
57. H. Takesue, N. Matsuda, E. Kuramochi, and M. Notomi, "Entangled photons from on-chip slow light," Sci. Rep. **4**, 3913 (2014).
58. S. Hughes, "Coupled-cavity QED using planar photonic crystals," Phys. Rev. Lett. **98**, 083603 (2007).
59. M. Minkov and V. Savona, "Radiative coupling of quantum dots in photonic crystal structures," Phys. Rev. B **87**, 125306 (2013).